2022 International Conference on Unmanned Aircraft Systems (ICUAS)
Dubrovnik, Croatia. June 21-24, 2022

Multidisciplinary Optimisation of an eVTOL UAV With a Hydrogen Fuel Cell

Bernardo Alves[1], André Marta[2] and Luís Félix[1]

2022 International Conference on Unmanned Aircraft Systems (ICUAS) | 978-1-6654-0593-5/22/$31.00 ©2022 IEEE | DOI: 10.1109/ICUAS54217.2022.9836228

***Abstract*— To explore the use of hydrogen fuel cells as a feasible alternative on Unmanned Aerial Vehicles (UAVs), a class I concept was designed at the Portuguese Air Force Research Centre (CIAFA). This work focuses on the Multidisciplinary Design Optimisation (MDO) methodology that was used to improve the 3h endurance of the baseline concept that had a Maximum Take-Off Weight of 21.6 kg, using 148 g of hydrogen and a 800 W fuel cell to power conventional flight operations. Another propulsive system comprised of batteries and rotors is used for Vertical Take-Off and Landing (VTOL). MDO was performed with the aid of OpenAeroStruct, a low fidelity software that combines Finite Element Analysis (FEA) and Vortex Lattice Method (VLM) to model lifting surfaces. Initially, a cruise and a load flight conditions were used with structural parameters and geometric twist as design variables. In a second approach, complexity was increased by including taper, wing chord and span as design variables in the problem formulation. Lastly, a third flight condition was introduced to ensure stall requirements were met. The use of MDO led to a 21% increase in endurance with a smaller wing, while satisfying all imposed constraints. This work marks an important milestone in the development of a future prototype at the CIAFA.**

I. Introduction

The use of hydrogen (H_2) as an alternative to fossil fuels is of interest to the defence sector. It is considered key for reaching the European Union goal of carbon neutrality and sustainability [1], [2]. So it becomes necessary to explore ways of using H_2. One possible use would be to power Unmanned Aerial Vehicles (UAVs).

Since 2009, starting with the project PITVANT [3], the Portuguese Air Force has developed and tested Unmanned Aircraft Systems (UAS) and thus acquired valuable know-how and experience in both the design and operation of class I vehicles. With the intent of exploring the application of fuel cells on UAVs and gain experience in the field of renewable energies, a project to design, build and later test an UAS prototype begun at the Portuguese Air Force Research Centre (CIAFA).

In the first phase of this project, the conceptual design, the design team used empirical formula of aircraft performance and a genetic algorithm to conduct optimal trade-off studies with respect to Maximum Take-Off Weight (MTOW) and endurance, resulting in a baseline concept with the desired compromise between the two [4]. Then, the design team used low fidelity software to validate the concept and further detail it. The proposed concept was used as a baseline for subsequent studies. This paper explains the Multidisciplinary Design Optimisation (MDO) approach chosen and presents a 2nd generation vehicle with extended endurance.

[1] Centro de Investigação da Academia da Força Aérea, Academia da Força Aérea, Instituto Universitário Militar, Granja do Marquês, 2715-021 Pêro Pinheiro, Portugal {bmalves,lffelix}@emfa.pt

[2] IDMEC, Instituto Superior Técnico, Universidade de Lisboa, Av. Rovisco Pais 1, 1049-001 Lisboa, Portugal andre.marta@tecnico.ulisboa.pt

II. The Baseline Concept

With the analytic hierarchy process (AHP) [5] and a set of defined criteria, a lift+cruise configuration was chosen. This type of configuration is characterised by having one or more propellers to provide the thrust needed in conventional flight, where the wing provides the lift needed, and several rotors to provide thrust in vertical take-off and landing (VTOL).

The UAV is equipped with two independent propulsive systems: one for conventional flight and the other for VTOL. A fuel cell with 800 W of nominal power is used together with a hydrogen tank, capable of storing 148 g of hydrogen, to power the first mode. The fuel cell converts the hydrogen into electric current to power the forward flight motor and UAV avionics. The VTOL is powered by Li-Po batteries due to the large power output required. Although the energetic density of batteries is much lower than hydrogen's and more weight is needed, they can provide high power outputs almost instantaneously while fuel cells cannot.

The proposed concept has four rotors and one propeller which is located in the aft of the fuselage. A twin boom is used to connect the wing to an inverted V-tail and to support the rotors. A representation of the concept is given in Fig. 1.

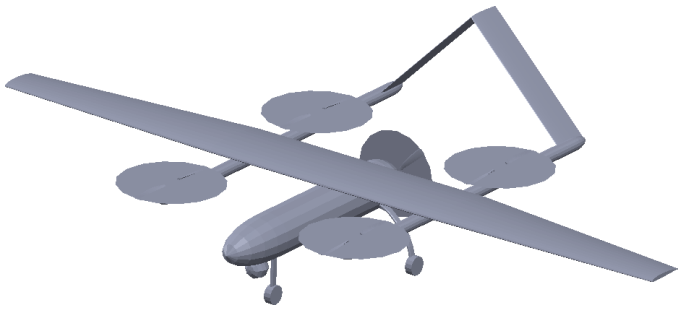

Fig. 1: CAD model of the lift+cruise proposed concept.

The main wing is composed of three panels. The centre panel is rectangular, with a constant chord of 0.399 m and span of 1.5 m. The two tip panels are tapered with $\lambda = 0.55$, each with a span of 1.25 m. The SG 6042 airfoil [6] was chosen for the entire wing which has a total span of 4.0 m. The geometry of the main wing is shown in Fig. 2.

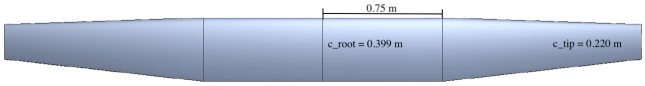

Fig. 2: Geometry of the main wing.

The inverted V-tail has a dihedral angle of -45º, a constant chord of 0.255 m, a projected span of 1.43 m using the NACA 0008 airfoil.

This hydrogen powered UAV will be used by the Portuguese Air Force to conduct surveillance missions, such as fire detection and incident control. Accordingly, the mission profile illustrated in Fig. 3 was defined.

The typical mission starts with vertical take-off, where the thrust required is provided by the rotors. After, transition between vertical and conventional modes occurs, accomplished by turning on the propeller while the rotors are still providing thrust. When enough forward speed is achieved, the rotors are shut down and the UAV will climb to reach the mission altitude to surveil a desired area or target. Afterwards, the UAV will return back to the starting point to start the descent phase. Close to the runway, a landing circuit will be performed before vertical descent which concludes the mission.

III. A Multidisciplinary Approach to Aircraft Design

Multidisciplinary Design Optimisation (MDO) methodologies have been used in the aerospace field for more than three decades. A survey of MDO methodologies and their application in the aerospace field is given in [7].

The use of MDO allows the designer to understand the trade-offs than exist among the different disciplines involved and explore them with numerical optimisation algorithms to achieve the best possible design for a given objective while satisfying the prevailing constraints. Two common applications of MDO in this field are simultaneous optimisation of aerodynamics-structures and simultaneous optimisation of structures-control. The coupling of aerodynamics and structures allowed designers to improve aircraft performance with the use of more efficient wings. For example, Grossman et al. [8] performed aerostructural optimisation of a sailplane and demonstrated that the designs obtained with MDO had a better performance than those obtained with sequential optimisation. In the aeronautical field, simultaneous structures-control optimisation can be used for active flutter suppression as demonstrated in [9] and in the space field for the reduction of vibrations in structures caused by, for example, the transition from the Earth's shade to sunlight [10], [11].

Although MDO had application potential, the cost of using such methodologies to solve complex problems with hundreds of design variables was often prohibitive due to the lack of computational power and the lack of efficient numerical methods. With both the development of more capable processors and the development of efficient gradient-based optimisation techniques, it is now possible to solve complex problems and obtain results in shorter time frames. Kenway and Martins [12] were able to perform aerostructural optimisation of a conventional transonic aircraft configuration using 476 design variables and eight different flight conditions using Euler CFD and a structural finite-element model within 36 hours. Still, the use of high-fidelity methods requires powerful dedicated machines with many processors which are not commonly available to students.

OpenAeroStruct [13], a lightweight open source software can provide fast results with a reasonable accuracy [14], hence it is appropriate to search the design space in the early design stages. Since it is open source, new features can be added to the source code to meet specific user needs. Chaudhuri et al. [15] used this tool to perform optimisation under uncertainty of a tailless aircraft and recently Ribeiro et al. [16] used it to build different surrogate models and assess their performance.

In this work, OpenAeroStruct was used to perform MDO of the main wing. It is a low-fidelity software which uses the Vortex Lattice Method (VLM) to determine the aerodynamic forces acting on lifting surfaces, and Finite-Element Analysis (FEA) to compute stresses and displacements on those same surfaces. It was developed using the NASA's OpenMDAO framework [17] to couple the aerostructural model and analytically calculate its derivatives to allow an efficient use of gradient-based algorithms.

OpenMDAO provides a modular environment to facilitate the integration of the different disciplines involved, each defined as an implicit function, later used in the unified derivatives equation to determine the total derivatives of the coupled model using the Modular-Analysis and Unified Derivatives (MAUD) architecture [18]. The developer defines each individual component, provides the partial derivatives of the outputs with respect to the inputs and makes the necessary connections to ensure a correct transfer of the coupling variables between them. OpenMDAO ensures the correct data flow between the different disciplines, which helps the developer to set up his/her own models. After the model has been set up, analysis and optimisation with the aid of gradient-based optimisation algorithms can be performed.

An illustration of the Vortex Lattice Method is provided in Fig. 4. It models each lifting surface as a thin plate subjected to a horseshoe vortex system. Each vortex filament induces a velocity at an arbitrary point P, as given by the Bio-Savart Law,

$$d\boldsymbol{V} = \frac{\Gamma}{4\pi} \cdot \frac{d\boldsymbol{l} \times \boldsymbol{r}}{|\boldsymbol{r}|^3}, \tag{1}$$

where Γ is the circulation strength, $\boldsymbol{r}$ is the distance between the vortex and P where the flow field is being assessed, and $d\boldsymbol{l}$ is the length of the vortex filament. Integration over a semi-infinite straight vortex yields

$$V = \frac{\Gamma}{4\pi h}, \tag{2}$$

with h being the distance between P and the start of the vortex filament. After establishing the relation between the

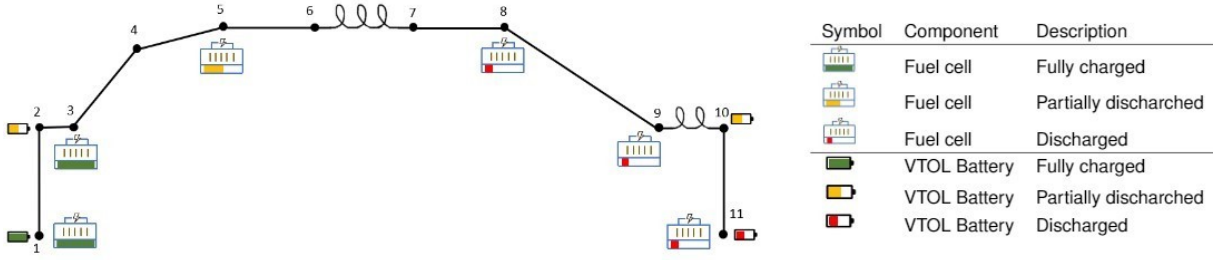

Fig. 3: Typical Mission Profile.

strength of the vortex and the induced speed, the flow tangency condition is imposed at all control points of each horseshoe vortex. This results in a system of linear equations of the form

$$\boldsymbol{A\Gamma} = -\boldsymbol{V}_\infty \cdot \boldsymbol{n}, \tag{3}$$

where $\boldsymbol{A}$ is the aerodynamic influence coefficient matrix and $\boldsymbol{V}_\infty$ represents the non-disturbed flow field. By solving this system, $\boldsymbol{\Gamma}$ is determined. Then, the aerodynamic forces acting on each panel are calculated as

$$\boldsymbol{F}_i = \rho\Gamma_i(\boldsymbol{V}_\infty + \boldsymbol{v}_i) \times \boldsymbol{l}_i. \tag{4}$$

Decomposing each one in the direction of the free-stream and its perpendicular, drag D and lift L contributions are estimated, respectively.

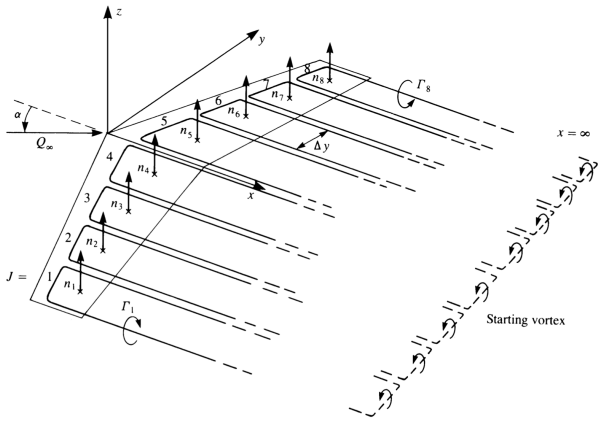

Fig. 4: Illustrative VLM model with multiple horseshoe vortices along the span [19]

The finite element analysis is performed using beam-bar elements with six degrees of freedom per node. The stiffness matrix for a single element is

$$\begin{bmatrix}
k_1 & 0 & 0 & 0 & 0 & 0 & -k_1 & 0 & 0 & 0 & 0 & 0 \\
0 & 12k_2^z & 0 & 0 & 0 & 6k_2^z l & 0 & -12k_2^z & 0 & 0 & 0 & 6k_2^z l \\
0 & 0 & 12k_2^y & 0 & -6k_2^y l & 0 & 0 & 0 & -12k_2^y & 0 & -6k_2^y l & 0 \\
0 & 0 & 0 & k_3 & 0 & 0 & 0 & 0 & 0 & -k_3 & 0 & 0 \\
0 & 0 & -6k_2^y l & 0 & 4k_2^y l^2 & 0 & 0 & 0 & 6k_2^y l & 0 & 2k_2^y l^2 & 0 \\
0 & 6k_2^z l & 0 & 0 & 0 & 4k_2^z l^2 & 0 & -6k_2^z l & 0 & 0 & 0 & 2k_2^z l^2 \\
-k_1 & 0 & 0 & 0 & 0 & 0 & k_1 & 0 & 0 & 0 & 0 & 0 \\
0 & -12k_2^z & 0 & 0 & 0 & -6k_2^z l & 0 & 12k_2^z & 0 & 0 & 0 & -6k_2^z l \\
0 & 0 & -12k_2^y & 0 & 6k_2^y l & 0 & 0 & 0 & 12k_2^y & 0 & 6k_2^y l & 0 \\
0 & 0 & 0 & -k_3 & 0 & 0 & 0 & 0 & 0 & k_3 & 0 & 0 \\
0 & 0 & -6k_2^y l & 0 & 2k_2^y l^2 & 0 & 0 & 0 & 6k_2^y l & 0 & 4k_2^y l^2 & 0 \\
0 & 6k_2^z l & 0 & 0 & 0 & 2k_2^z l^2 & 0 & -6k_2^z l & 0 & 0 & 0 & 4k_2^z l^2
\end{bmatrix} \tag{5}$$

where $k_1 = \frac{EA}{L}$, $k_2^z = \frac{EI_z}{L^3}$, $k_2^y = \frac{EI_y}{L^3}$, $k_3 = \frac{GJ}{L}$ and E is the Young's modulus, A is the beam cross sectional area, L is length, G is the shear modulus, J is the polar moment of inertia and I_s are the second moment of area about each axis.

After the assembly of the global stiffness matrix $\boldsymbol{K}$, the linear system of equations

$$\boldsymbol{Ku} = \boldsymbol{f} \tag{6}$$

is solved for the vector of displacements $\boldsymbol{u}$ given the applied aerodynamic nodal forces $\boldsymbol{f}$. To determine the stiffness matrix for each element, the cross-section properties are needed. To compute them, a wingbox model is used, which allows the use of the spar and skin thicknesses as design variables in the optimisation problem. The position of the front and rear spars are user-defined based on the airfoil coordinates. Along the wingspan, these coordinates are scaled with the local chord but their relative distance remains fixed.

The major limitations with this model are: the same thickness is used for both the front and rear spars and the same thickness is used for the upper and lower skins; it is not possible to use different airfoils along the wingspan. A detailed description of this model can be found in [14].

The lifting surfaces cause disturbances in the flow field and therefore are subject to aerodynamic forces, which cause stress and displacement on the structure. The deformed shape induces new disturbances in the flow and the aerodynamic forces generated are different. To ensure the coupling of these two disciplines, it is required to transfer the aerodynamic loads to the structures and determine the displacements and stresses they produce until

$$\boldsymbol{\mathcal{R}}_i(\boldsymbol{y}, \boldsymbol{y}^t) = 0, \tag{7}$$

i.e, when the target $\boldsymbol{y}^t$ and the state $\boldsymbol{y}$ variables match. OpenMDAO has several solvers that can be used to converge the model. After the multidisciplinary analysis, the objective and constraints of the optimisation problem can be evaluated. The extended design structure matrix (XDSM) [20] of the aerostructural model is provided in Fig. 5.

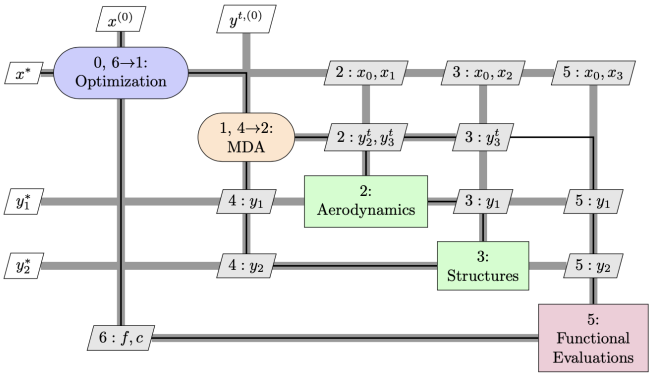

Fig. 5: XDSM diagram of the default aerotsructural optimisation problem in OpenAeroStrcut [13].

The load and transfer scheme implemented in OpenAeroStruct is both consistent and conservative [13]. The process is simplified by using the same discretisation for both the elements of the FEA and the VLM mesh.

To use the wingbox model, the shear centre location is estimated as the average of the location of the spars weighted by their respective area [14].

The baseline UAV is to be used to conduct surveillance missions. As such, the objective of the optimisation is to extended its endurance, given a set of constraints. Because it is an electric aircraft powered by batteries, motors and a fuel cell, the weight variation in flight is negligible when compared to the MTOW. The endurance equation [21]

$$E = \frac{L}{D}\frac{E_{sb}\eta_{b2s}\eta_p}{(W_0 + W_s)V_\infty}m_b \tag{8}$$

was added to the Functional Evaluations of OpenAeroStruct (refer to Fig. 5) where E_{sb} is the battery specific energy in W.h/kg, η_{b2s} the system efficiency from battery to motor output shaft, η_p the propeller efficiency, m_b the battery mass in kg, W_0 the aircraft empty weight and W_s the structural weight. The total energy content given by $E_{sb} \cdot m_b$ in (8) was replaced by the product of the available hydrogen mass for the cruise segment and hydrogen's specific energy

$$E_{total} = m_{H_2 avail} \cdot e. \tag{9}$$

First, an OpenMDAO ExplicitComponent class was created. In its definition, the partial derivatives of endurance with respect to each of the inputs were provided. The partial derivatives were calculated using analytic methods. Afterwards, an object from this class was instantiated inside the *total_perf*, which is a class defining an OpenMDAO Group. Some parameters such as the efficiencies η_{b2s}, η_p and the total energy content as given by (9) were assumed constant during the optimisation process and stored inside the *prob_vars* component. The other variables such as L, D and W_s are already calculated by other components in OpenAeroStruct, therefore it was necessary to connect them to this new component. An illustrative N2 diagram with the *endurance* component expanded is provided in Fig. 6. Its inputs are represented in orange and the outputs in green.

There are several standard OpenAeroStruct geometric manipulation functions that can be used to define the initial shape of lifting surfaces and also modify them during optimisation. An example of such function is the *Taper*, which can be used to decrease the chord linearly from root to tip, producing a tapered wing. A transformation about the quarter-chord line. A new taper function was sought to decrease the chord linearly from a user-defined position until the tip, while keeping the leading edge perpendicular to the fuselage. A bottom-up approach was used. First, a new OpenMDAO ExplicitComponent class was defined: the user inputs are the ratio $\lambda = \frac{c_{tip}}{c_{root}}$ and an offset which should be given as a percentage of the semi-span; the output is the altered mesh. The partial derivatives of the output (mesh) with respect to the inputs (taper and offset) were defined analytically. A simplification was made: the partial derivative of the mesh with respect to the offset was set to 0, i.e the offset cannot be used as design variable in the optimisation problem. An illustrative N2 diagram of this new *taper_with_offset* geometric function is provided in Fig. 7. With this new feature, the definition of a general trapezoidal lifting surface is easier. Also, the use of λ as design variable is possible without affecting the constant chord segments of the lifting surfaces.

IV. Next Generation UAV Concept

As stated previously, the goal of using MDO is to extend the baseline endurance while satisfying the constraints.

Initially, the aerostructural problem was comprised of two distinct flight conditions: one corresponding to the main surveillance mission where the objective function is to be maximised; and another for a 6.0 g load case to safely size the structure of the main wing. Two lifting surfaces were defined, wing and tail, assumed built of a composite material made from a mixture of bidirectional carbon fibre and epoxy resin [22]. The structures were modelled as simplified wingboxes, with the front spar at 10% of the chord and the rear one at 60%. The geometry of each box was based on the coordinates of the selected airfoils for the wing and tail, SG 6042 and NACA 0008, respectively. A summary of the these properties is provided in Tab. I.

To ensure that the UAV is in trimmed level flight, the constraints $L = W$ and $C_M = 0$ were added to the main mission. In the manoeuvre case, only the former is imposed. At this flight condition, a failure constraint based on the von Mises stresses aggregated with a Kreisselmeier–Steinhauser (KS) function [23] must also be satisfied. Finally, a monotonic constraint was imposed to the geometric twist.

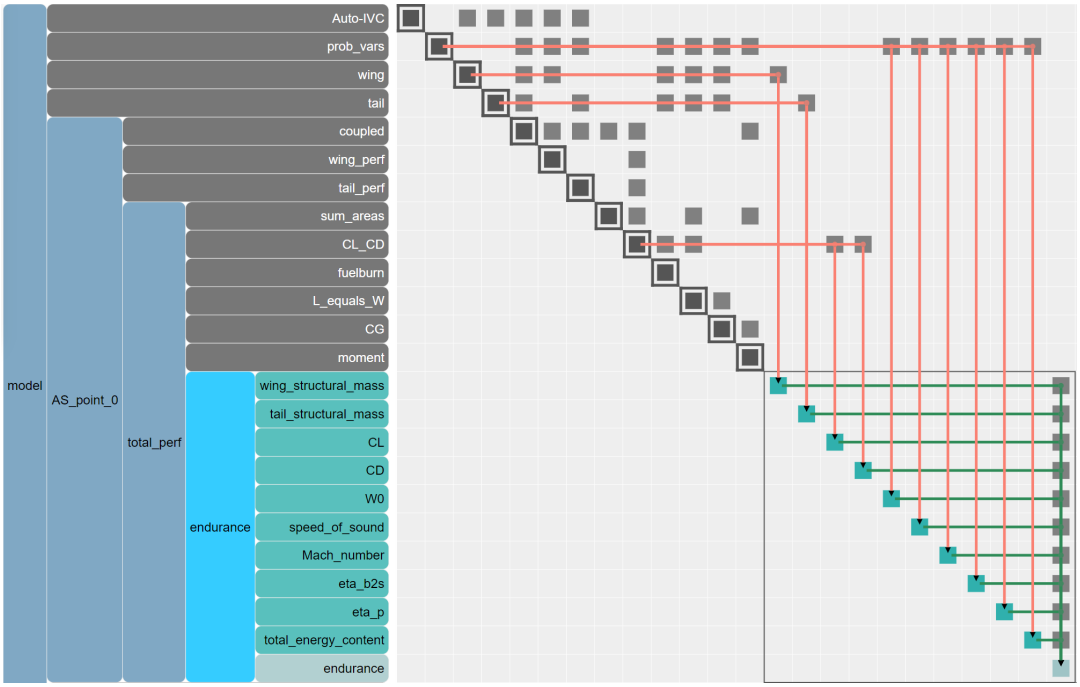

Fig. 6: N2 diagram of the model with *endurance* inputs/outputs highlighted.

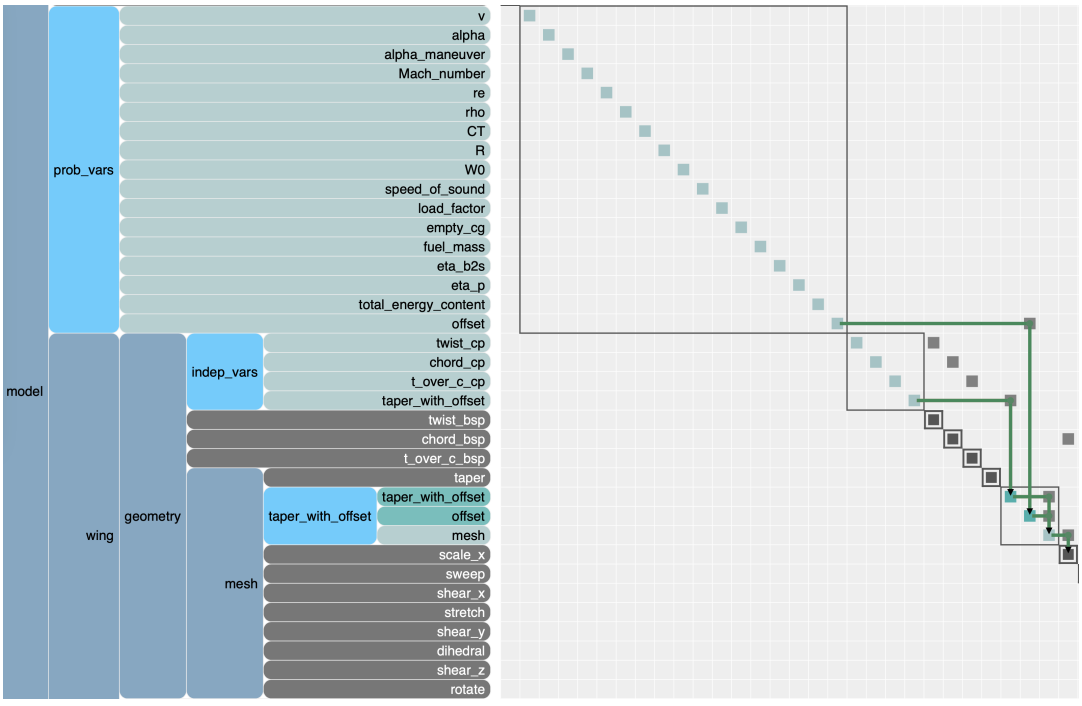

Fig. 7: N2 diagram of the model with *taper_with_offset* inputs/outputs evidenced.

TABLE I: Parameters and specifications of the baseline UAV.

Parameter	Value	Notes
Tank capacity	148 g of H_2	Maximum hydrogen stored
Energy	3479.85 W.h	Total energy available for main mission
MTOW	21.6 kg	
Main mission Mach	0.05647	
Main mission altitude	5000 ft	ISA + 20° C
6.0 g manoeuvre Mach.	0.07331	According to UAV's flight envelope
6.0 g manoeuvre altitude	0 ft	ISA + 20° C
Drag counts for VTOL rotors	350	
Aircraft weight without wing and tail structures	17.118 kg	
Structural material density	1300 kg/m^3	Based on bidirectional carbon fabric + epoxy
Structural Young's modulus	48.99 MPa	Based on bidirectional carbon fabric + epoxy
Structural shear modulus	5 GPa	Based on bidirectional carbon fabric + epoxy
Structural yield strength	567.79 MPa	Based on bidirectional carbon fabric + epoxy

The design variables of the optimisation problem are: the wing geometric twist, spar and skin thicknesses, which are parametrised with b-splines; the angle of attack of the manoeuvre $\alpha_{6.0g}$ and main mission α cases, and the tail incidence angle α_i, which are scalars. The lower and upper bounds for the wing twist, spar and skin thicknesses are -15° and 15°, 0.6 and 3 mm, respectively. A summary of the optimisation problem is given in Tab. II.

The algorithm chosen was the SLSQP (Sequential Linear Squares Programming) [24] available in the Python library *SciPy* [25], with a tolerance set to 10^{-7} and 200 maximum iterations as fallback.

To choose the number of VLM panels, aerodynamic analyses of both lifting surfaces were conducted. During the analyses, the aerodynamic efficiency L/D was observed against the number of panels. A compromise between precision of the numerical solution and computational time was achieved with 200 panels on each wing, each cross section with 5 chord-wise nodes.

Before proceeding with the optimisation, the baseline model was run to determine its performance, using only α, $\alpha_{6.0g}$ and α_i to obtain a trimmed level flight condition. For a cruise speed of 38 kts, the obtained endurance of the baseline was 3h29 at 21.6 kg of MTOW. This speed was kept fixed during all subsequent optimisations.

A. Optimisation With Geometric Twist

With the optimisation problem defined in Tab. II and the termination criteria defined, the program was executed. After 16 iterations, a solution was found, while satisfying all constraints. The obtained parameter distributions along the wingspan and tailspan are provided in Fig. 8a and 8b, respectively.

Because the wing twist was given as design variable, the introduction of wash-out was expected to reduce the lift-induced drag. A reduction in this drag contribution will increase the aerodynamic efficiency L/D and improve the endurance as given by (8).

The von Mises stresses on the wing and tail structures are lower than the allowable stress limit, represented in red.

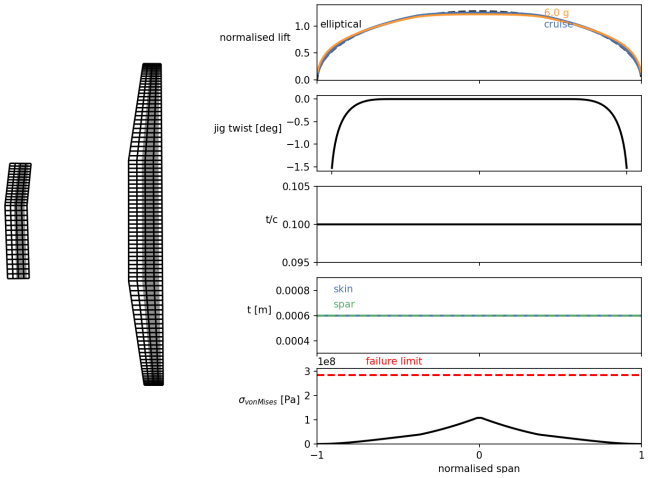

(a) Wing

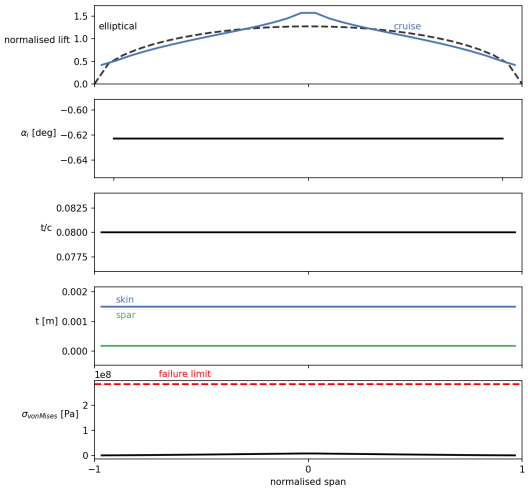

(b) Tail

Fig. 8: Optimised parameter distribution along wingspan.

Hence, failure is not expected.

The obtained endurance was barely higher than the base-

TABLE II: Optimisation problem.

	Function/variable	Note	Quantity
maximise	endurance	computed using (8)	
with respect to	wing twist (case A. only)	b-spline parametrised using 5 control points	5
	wing taper λ (case B. only)		1
	wing root chord c_{root} (case B. only)		1
	wingspan b (case B. only)		1
	spar thickness	b-spline parametrised using 6 control points	6
	skin thickness	b-spline parametrised using 6 control points	6
	α	for the main mission	1
	α_i	for the main mission	1
	$\alpha_{6.0\,\mathrm{g}}$	for the 6.0 g load case	1
		Total design variables	**20**
subject to	$L = W$	for the main mission	1
	$C_M = 0$	in the main mission to ensure trimmed flight	1
	$L_{6.0\,\mathrm{g}} = W_{6.0\,\mathrm{g}}$	for the 6.0 g manoeuvre flight point	1
	$\sigma_{\text{von Mises}} \leq \frac{\sigma_{\text{yield}}}{2}$	von Mises stresses aggregated using a KS function	1
	$TA_{\text{monotonic}} < 0$	monotonic twist constraint	1
		Total constraint functions	**5**

line, just improving 0.03%. Also, it was verified that the optimal solution had worse aerodynamic efficiency when compared to the original concept: L/D was 14.24 in the baseline and it decreased to 13.1 in the optimised solution. The increase in endurance was accomplished by a reduction of the weight of the structures, W_s. In fact, W_s is the lowest possible for this problem formulation, since both structural design variables correspond to the lower bounds.

The reduction in the structural weight will impact the flight conditions. Because the flight speed V is fixed, to satisfy the equilibrium constraint $L = W$ the angle of attack α has to decrease. Flying at lower angles of attack will decrease both lift and drag, but this reduction does not necessarily imply higher values of L/D. If lift reduces more than drag, then the aerodynamic efficiency will decrease. This suggested that, with a weight reduction, it might be possible to fly at speeds lower than the defined 38 kts and achieve higher endurance. Nonetheless, because there was no intention on flying with lower speeds than the defined 38 kts due to operational requirements, planform design variables were introduced. By allowing the planform to change, it was expected to obtain a wing with lower area such that:

1) the structural weight W_s further decreases;
2) the flight angle of attack α and consequently L/D increase.

B. Optimisation With Taper, Root Chord and Wingspan

After experimenting with geometric twist, this parameter was fixed at 0 and taper was used. As described in Section III, the linear reduction of chord can start at an arbitrary position on the lifting surface. To study the impact that this location would have on both aerodynamic and structural parameters, parametric studies were performed: 3 optimisations were performed in total, each with a different taper offset. From these studies, it was noted that the optimiser was driving the ratio λ to the lower bound to reduce the wing area S_{wing} as much as possible. The solution with the lowest area had the highest endurance.

Later, the root chord was added to the set of design variables of the optimisation problem and the design framework was executed again. The result was a smaller wing, achieved with $\lambda = 0.23$ and $c_{root} = 0.196\,\mathrm{m}$. Smaller wings were not possible for the given flight conditions because the angle of attack α was already at the defined upper bound of 10.0º.

Finally, the wing span b was added as well and the design framework was re-executed. The result was a wing with a higher aspect ratio, which was accomplished by an increase of the span. The flight angle of attack α was again at the upper bound. A summary of the results obtained is provided in Tab. III.

Every time a new design variable was added to the problem formulation, the endurance improved and some patterns could be identified:

1) smaller wings had higher aerodynamic efficiency L/D and lower structural weight W_s and, hence, higher endurance as given by (8);
2) the angle of attack α was constraining the area reduction of the lifting surface.

The first point enumerated above could be explained by how drag is estimated in OpenAeroStruct,

$$D = \frac{1}{2}\rho V_\infty^2 S_{ref}(C_{D_0} + C_{D_i} + C_{D_v} + C_{D_w}), \qquad (10)$$

where C_{D_0} was used to account for the drag contribution of components that are not modelled in the analysis such as vertical rotors, fuselage, double-boom and landing gear; C_{D_i} is the lift-induced drag component; C_{D_v} is the viscous drag contribution, estimated based on flat-plate empirical formulations [21, sec. 12.5.3]; and C_{D_w} is the wave drag as given by the Korn equation [26]. Of all contributions,

C_{D_0} is the largest and was assumed constant. This value was estimated conservatively due to the disturbances that the vertical flight rotors will induce on the incoming airflow. Different lift distributions will contribute differently to the lift-induced drag coefficient C_{D_i}, nonetheless because $C_{D_0} >> C_{D_i}$, the lift distribution along the wingspan will not substantially affect the total drag D. Following the same logic, variations of the angle of attack α will alter the lift-induced drag coefficient C_{D_i} but will not have much effect on the total drag D. Hence, reducing the wing area S_{wing} will contribute to a decrease in the reference area S_{ref} in (10), and ultimately contribute to reduce the total drag D, even though higher angles of attack will be needed to satisfy the equilibrium constraint $L = W$.

The second pattern identified is related to a missing stall constraint in the problem formulation given in Tab. II. The optimisation algorithm exploits the lack of a stall constraint to reduce the wing area as much as possible and maximise endurance. As a result, it might be possible that the UAV will stall before the defined upper bound for the cruise flight speed defined. If it happens, the solutions found would be unfeasible.

C. Stall Considerations

To verify if stall occurs, first the maximum 2D lift coefficient of the wing airfoil was determined. XFOIL [27], [28] was used to conduct aerodynamic analyses of the SG 6042 airfoil at different Reynolds number Re and Ncrit – a parameter used for predicting transition – set to 5 and 9. It was verified that the maximum lift coefficient $C_{l_{2D}}$ was between 1.4 and 1.5. The data corresponding to the optimal solutions found with the planform design variables was post-processed and the sectional lift coefficient at cruise conditions along the wingspan was produced in Fig. 9a. It was observed that two of the solutions found would stall at the defined cruise speed.

Therefore, a new constraint was added at the main mission

$$C_l < C_{l_{2D}} \tag{11}$$

and the design framework was again executed with wing taper and root chord as design variables and, afterwards, with span as well. Since this C_l constraint was active, it was expected that the results of these two optimisations would be different, as demonstrated in Fig. 9b.

With the addition of the constraint, the angle of attack α was no longer at the upper bound and the wing area S_{wing} increased, which resulted in worse endurance. The results with and without the C_l constraint, for the cases where it was active, are also summarised in Tab. III.

D. Final Optimal Solution

Although a stall constraint had been successfully implemented in the optimisation problem and feasible solutions had been found, the stall speed requirement which was set in the beginning of this project,

$$V < 28\,kts, \tag{12}$$

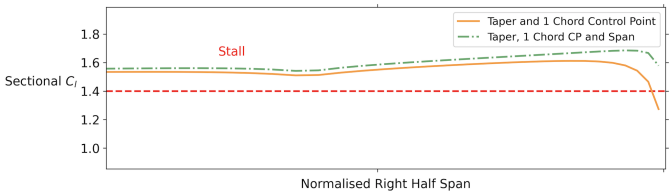

(a) Without stall constraint.

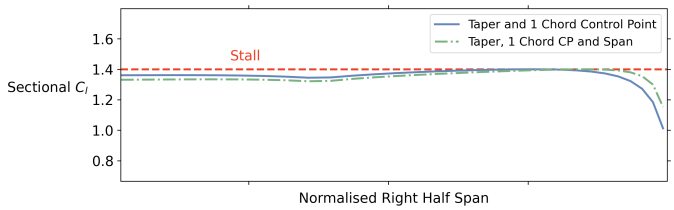

(b) With stall constraint.

Fig. 9: Sectional lift coefficients at cruise conditions.

is not satisfied, since at the cruise speed $C_l = C_{l_{2D}}$ for some sections of the wings that were obtained previously.

In order to ensure that the requirement given in (12) is respected, a third flight condition was introduced in the optimisation problem where the C_l constraint as given by (11) was imposed. Similarly to the cruise condition, no loads were applied and it was ensured that the lift being generated would be equal to the weight of the vehicle.

The design framework was executed, and after 25 iterations the optimisation algorithm was able to find an optimal solution satisfying all constraints. Compared to the baseline model, the wing area S_{wing} decreased, the taper ratio λ and the wing root chord reduced, and finally the span b increased. Because the stall constraint was imposed at a lower speed, the area of the lifting surface did not reduce as much as when the constraint was imposed at the cruise speed. A summary of the results obtained is provided in Tab. III, together with the results of all other cases for comparison purposes.

Similar to the previous results, the optimisation algorithm reduced the wing area as much as possible being the stall constraint the one that limited this reduction. The sectional lift coefficient for this improved solution at a stall speed of 28 kts is provided in Fig. 10.

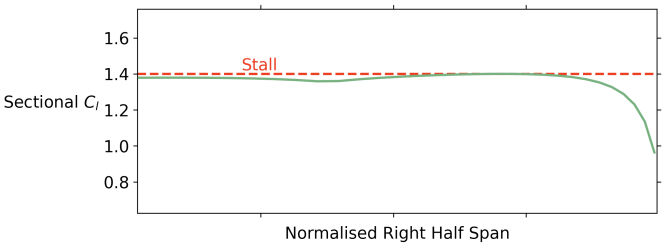

Fig. 10: Sectional lift coefficients at the defined stall speed.

It is observed that the maximum C_l value is reached between 50 and 75% of the semi-span.

TABLE III: Comparison between optimal solutions.

	baseline	wing twist	with taper and chord		with taper, root chord and span		w. 3 flight cases	
Parameter	Value	Value	Value[a]	Value	Value[a]	Value	Value	Unit
Endurance	03:29	03:35	05:13	05:29	05:20	05:41	04:14	h:min
C_L	0.601	0.536	0.813	0.868	0.814	0.890	0.630	-
C_D	0.042	0.041	0.044	0.045	0.043	0.044	0.041	-
L/D	14.24	13.1	18.3	19.1	19.0	20.4	15.2	-
MTOW	21.6	19.4	18.63	18.57	19.0	19.1	19.0	kg
W_s	4.98	2.8	2.02	1.95	2.36	2.43	2.41	kg
α	3.28	2.4	8.40	10.0	8.0	10.0	3.9	deg
$\alpha_{6.0g}$	11.0	10.6	20.8	23.7	20.1	23.9	12.6	deg
α_i	-1.1	-0.8	-3.8	-4.7	-3.6	-4.9	-1.5	deg
c_{root}	0.399	0.399	0.210	0.196	0.186	0.166	0.272	m
λ	0.55	0.55	0.37	0.23	0.25	0.1	0.44	-
b	4.0	4.0	4.0	4.0	4.9	5.0	4.7	m
S_{wing}	1.373	1.373	0.677	0.596	0.696	0.598	1.057	m^2

[a]with C_l constraint

The structural design variables, namely, the skin and spar thicknesses correspond approximately to the lower bound defined: 0.6 mm. The exact variation of these parameters along the wingspan and the corresponding von Mises stresses are provided in Fig. 11.

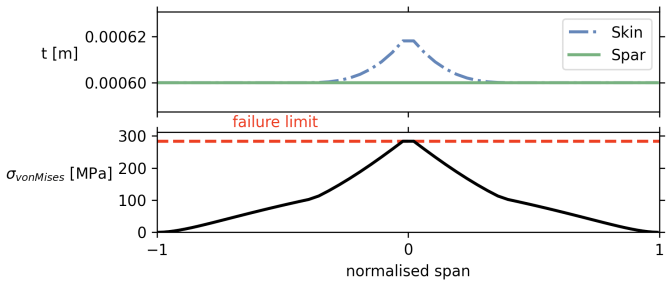

Fig. 11: Optimised parameter distribution obtained with three flight conditions.

The spar thickness is constant and equal to the lower bound, but the skin thickness has a small variation. It is larger at the wing root where the stresses are higher, and smaller towards the tips where they are lower. Because the allowable stress is reached at the wing root, it was not possible to obtain smaller thickness values.

The total endurance of the UAV increased from 3h35 to 4h15, which represents an increase of 21%.

V. Conclusions

This work focused on employing Multidisciplinary Design Optimisation to improve the baseline concept of a small electric UAV with VTOL capability, powered by a hydrogen fuel cell, with the goal of extending its endurance.

First, some features were added to OpenAeroStruct to calculate the objective function and allow the definition of general planform shapes. To improve the computational efficiency of the optimisation process, analytical partial derivatives were defined for these new components.

Afterwards, improvements to the baseline were sought. Initially, structural parameters such as the skin and spar thicknesses, as well as geometric twist were used as design variables. The use of geometric twist was not sufficient to improve the baseline concept.

Therefore, more design variables were added. Instead of using geometric twist, taper was used with different offsets. After the trends had been analysed, the chord of the inboard section of the wing was allowed to change and the design framework was executed. Lastly, the wingspan was added to the set of design variables. By allowing the wing planform shape to change, some common trends were observed: the wing area was being reduced; and the aspect ratio was being increased.

Through analysis of the results of the different optimisation runs it was found that the lack of a stall constraint allowed the optimisation algorithm to make considerable reductions of the wing area and use high angles of attack to satisfy the equilibrium of forces. Therefore, a stall constraint was introduced in the problem formulation. Because it was active for some of the previous solutions, changes in the optimal solutions were expected. Even though the same trends were verified, the area of the wing did not reduce as much when compared to the cases when no stall constraint existed.

Finally, to satisfy the stall speed requirement given in (12), a third flight condition at 28 kts was introduced in the problem formulation. No loads were applied and both the equilibrium and stall constraints were imposed. Compared to the baseline, the result was a smaller wing with higher aspect ratio which resulted in 21% more endurance. Other solutions with extended endurance were found but they do not satisfy this last constraint.

References

[1] European Union, "Long-term low greenhouse gas emission development strategy of the european union and its member states," March 2020. [Online]. Available: https://unfccc.int/documents/210328

[2] P. Edwards, V. Kuznetsov, W. David, and N. Brandon, "Hydrogen and fuel cells: Towards a sustainable energy future," *Energy Policy*, vol. 36, no. 12, pp. 4356–4362, 2008, foresight Sustainable Energy Management and the Built Environment Project.

[3] J. Morgado and J. Sousa, "O programa de investigação e tecnologia em veículos aéreos autónomos não tripulados da academia da força aérea," *IDN Cadernos*, vol. II Série, no. 4, pp. 9–24, 2009. [Online]. Available: https://www.idn.gov.pt/pt/publicacoes/idncadernos/Documents/2009/caderno4_II.pdf

[4] B. Alves, V. Coelho, P. Silva, A. Marta, F. Afonso, P. Sá, L. Félix, and J. Caetano, "Design of a hydrogen powered small electric fixed-wing uav with vtol capability," in *International Conference on Multidisciplinary Design Optimization of Aerospace Systems*, A. C. Marta and A. Suleman, Eds., ECCOMAS. Lisbon, Portugal: IDMEC, IST, July 2021, pp. 290–304, ISBN: 978-989-99424-8-6. [Online]. Available: https://www.eccomas.org/wp-content/uploads/sites/15/2021/11/AeroBest2021_proceedings-1.pdf

[5] T. L. Saaty and L. G. Vargas, *Models, Methods, Concepts & Applications of the Analytic Hierarchy Process*, 2nd ed., ser. International Series in Operations Research & Management Science. Springer, 2012.

[6] P. Giguère and M. S. Selig, "New Airfoils for Small Horizontal Axis Wind Turbines," *Journal of Solar Energy Engineering*, vol. 120, no. 2, pp. 108–114, 1998.

[7] J. Sobieszczanski-Sobieski and R. T. Haftka, "Multidisciplinary aerospace design optimization: survey of recent developments," *Structural optimization*, vol. 14, no. 1, pp. 1–23, Aug 1997. [Online]. Available: https://doi.org/10.1007/BF01197554

[8] B. Grossman, Z. Gurdal, G. J. Strauch, W. M. Eppard, and R. T. Haftka, "Integrated aerodynamic/structural design of a sailplane wing," *Journal of Aircraft*, vol. 25, no. 9, pp. 855–860, 1988. [Online]. Available: https://doi.org/10.2514/3.45670

[9] S. Suzuki and S. Matsuda, "Structure/control design synthesis of active flutter suppression system by goal programming," *Journal of Guidance, Control, and Dynamics*, vol. 14, no. 6, pp. 1260–1266, 1991. [Online]. Available: https://doi.org/10.2514/3.20782

[10] S. L. Padula and C. A. Sandridge, *Passive/Active Strut Placement by Integer Programming*. Dordrecht: Springer Netherlands, 1993, pp. 145–156. [Online]. Available: https://doi.org/10.1007/978-94-011-1804-0_12

[11] U. Hirsch, H.-B. Kuntze, R. Brecht, and A. Kilthau, "Structure and parameter optimization of an active adsorber for decentralized vibration control," in *Proceedings 1992 IEEE International Conference on Robotics and Automation*, 1992, pp. 670–675 vol.1.

[12] G. K. W. Kenway and J. R. R. A. Martins, "Multipoint high-fidelity aerostructural optimization of a transport aircraft configuration," *Journal of Aircraft*, vol. 51, no. 1, pp. 144–160, 2014. [Online]. Available: https://doi.org/10.2514/1.C032150

[13] J. P. Jasa, J. T. Hwang, and J. R. R. A. Martins, "Open-source coupled aerostructural optimization using python," *Structural and Multidisciplinary Optimization*, vol. 57, no. 4, pp. 1815–1827, 2018.

[14] S. S. Chauhan and J. R. R. A. Martins, "Low-fidelity aerostructural optimization of aircraft wings with a simplified wingbox model using openaerostruct," in *EngOpt 2018 Proceedings of the 6th International Conference on Engineering Optimization*, H. Rodrigues, J. Herskovits, C. Mota Soares, A. Araújo, J. Guedes, J. Folgado, F. Moleiro, and J. F. A. Madeira, Eds. Cham: Springer International Publishing, 2019, pp. 418–431.

[15] A. Chaudhuri, J. Jasa, J. R. R. A. Martins, and K. E. Willcox, *Multifidelity Optimization Under Uncertainty for a Tailless Aircraft*. [Online]. Available: https://arc.aiaa.org/doi/abs/10.2514/6.2018-1658

[16] C. Ribeiro, F. Afonso, M. Sohst, and A. Suleman, "Surrogate-based multidisciplinary design optimization of an uam-vtol aircraft for energy minimization," in *International Conference on Multidisciplinary Design Optimization of Aerospace Systems*, A. C. Marta and A. Suleman, Eds., ECCOMAS. Lisbon, Portugal: IDMEC, IST, July 2021, pp. 79–97, ISBN: 978-989-99424-8-6. [Online]. Available: https://www.eccomas.org/wp-content/uploads/sites/15/2021/11/AeroBest2021_proceedings-1.pdf

[17] J. S. Gray, J. T. Hwang, J. R. R. A. Martins, K. T. Moore, and B. A. Naylor, "OpenMDAO: An open-source framework for multidisciplinary design, analysis, and optimization," *Structural and Multidisciplinary Optimization*, vol. 59, no. 4, pp. 1075–1104, 2019.

[18] J. T. Hwang and J. R. R. A. Martins, "A computational architecture for coupling heterogeneous numerical models and computing coupled derivatives," *ACM Transactions on Mathematical Software*, vol. 44, p. Article 37, 2018.

[19] J. Katz and A. Plotkin, *Low-speed aerodynamics*. Cambridge university press, 2001, vol. 13.

[20] A. B. Lambe and J. R. R. A. Martins, "Extensions to the design structure matrix for the description of multidisciplinary design, analysis, and optimization processes," *Structural and Multidisciplinary Optimization*, vol. 46, no. 2, pp. 273–284, 2012.

[21] D. P. Raymer, *Aircraft Design: A Conceptual Approach*. American Institute of Aeronautics and Astronautics, Inc, 1992.

[22] J. Silva, "Design and optimization of a wing structure for a uas class i 145 kg," Master's thesis, Academia da Força Aérea, Sintra, Portugal, 2017. [Online]. Available: http://hdl.handle.net/10400.26/23156

[23] G. Kreisselmeier and R. Steinhauser, "Systematic control design by optimizing a vector performance index," *IFAC Proceedings Volumes*, vol. 12, no. 7, pp. 113–117, 1979, iFAC Symposium on computer Aided Design of Control Systems, Zurich, Switzerland, 29-31 August.

[24] D. Kraft, "A software package for sequential quadratic programming," DLR German Aerospace Center – Institute for Flight Mechanics, Koln, Germany, Tech. Rep. DFVLR-FB 88-28, July 1988.

[25] P. Virtanen, R. Gommers, T. E. Oliphant, M. Haberland, T. Reddy, D. Cournapeau, E. Burovski, P. Peterson, W. Weckesser, J. Bright, S. J. van der Walt, M. Brett, J. Wilson, K. J. Millman, N. Mayorov, A. R. J. Nelson, E. Jones, R. Kern, E. Larson, C. J. Carey, İ. Polat, Y. Feng, E. W. Moore, J. VanderPlas, D. Laxalde, J. Perktold, R. Cimrman, I. Henriksen, E. A. Quintero, C. R. Harris, A. M. Archibald, A. H. Ribeiro, F. Pedregosa, P. van Mulbregt, and SciPy 1.0 Contributors, "SciPy 1.0: Fundamental Algorithms for Scientific Computing in Python," *Nature Methods*, vol. 17, pp. 261–272, 2020.

[26] B. Malone and W. H. Mason, "Multidisciplinary optimization in aircraft design using analytic technology models," *Journal of Aircraft*, vol. 32, no. 2, pp. 431–438, 1995.

[27] M. Drela, "An analysis and design system for low reynolds number airfoils," in *Conference on Low Reynolds Number Airfoil Aerodynamics*. University of Notre Dame, 1989.

[28] M. Drela and H. Youngren, *XFOIL 6.9 User Primer*, 2001.